ISSN: 2688-8645

Parametric Study on Separation Performance of a New Downhole Sand Retrieval Device

Hao Wang, Zhewei Ye, Bing Liu, Changjiang Li

School of Mechanical Engineering, Southwest Petroleum University, Chengdu, Sichuan, 610500, China

Abstract

The paper addresses the conditions of oil and gas wells with high sand content, low formation pressure coefficients, and high loss rates, where existing sand removal methods are inefficient. A novel sand-bailing device that is both fast and efficient has been designed. Its innovation lies in the design of a separation hood structure for sand and water separation within the cylinder, which enables direct and rapid sand removal. This paper investigates the various parameters affecting the separation efficiency of the novel sand-bailing device under transient conditions using computational fluid dynamics (CFD) methods, specifically employing the Euler model and the standard k-ε turbulence model. The simulation results were validated by comparing them with experimental results, confirming the accuracy and reliability of the simulations. The results indicate that the parameters affecting the separation efficiency of the device include the length of the inlet pipe, the diameter of the separation hood, the drilling speed, the inlet flow rate, the drilling fluid viscosity, and the sand particle size, and that the extent of their impact on the device's separation efficiency varies. The research findings provide valuable theoretical guidance for the structural design and separation performance study of the novel sand-bailing device.

Keywords

Novel Sand-bailing Device; Separation Hood; Computational Fluid Dynamics; Euler Model; Separation Efficiency.

1. Introduction

Sand production occurs not only in gas hydrate wells and water wells [1], but also in many gas and oil wells. The hazards and impacts of sand production in oil and gas wells involve many aspects of oilfield operations [2]. Scientifically sound techniques should be developed for oil and sand prevention based on actual conditions to achieve effective sand removal and prevention [3]. Therefore, the study of downhole desanding equipment has become a hot issue in oil and gas extraction [4]. Currently, the sand removal technologies addressing these problems in oil and gas wells mainly include mechanical sand extraction, circulating sand flushing, continuous tube negative pressure sand flushing, and other sand removal technologies [5, 6]. Zhang et al. modified the conventional sand dredging process by adding a multi-stage single-flow valve to the sand-sedimentation tailpipe, creating a high-efficiency, low-injury, negative-pressure, sand dredging process for horizontal wells [7]. Concentric pipe jet negative pressure sand flushing technology has been researched in Xinjiang Oilfield in China [8]. Multiple companies, including Schlumberger, have conducted research on continuous sand-flushing technology and have developed relatively mature continuous sand-flushing and well-cleaning techniques [9, 10, 11]. In addition, vacuum sand extraction technology has been successfully applied to sand removal operations under low-pressure conditions abroad [12].

ISSN: 2688-8645

The core of sand removal operations lies in the separation of sand and liquid. Many scholars have already conducted extensive analysis and research on the two-phase flow and separation of particles. Liu et al. conducted numerical simulations and found the simultaneous existence of particles moving in both axial and radial directions in a vertical pipe [13]. Li and Wang [14, 15] conducted sand-carrying tests on vertical wellbores and obtained the parameters affecting the settling velocity of sand particles. Park et al. [16] used Eulerian multiphase flow to predict the settling of solids. Severino et al. developed mechanical models for solid-liquid hydrocyclones to describe the separation efficiency curves [17]. Huang et al. performed numerical simulations of solid-liquid separation in a horizontal spiral sedimentation centrifuge and analyzed the effects of operating speed and flow rate on the separation efficiency [18]. Kamyab and Rasouli investigated the effect of different parameters on rock chip transportation through numerical simulations of computational fluid dynamics using the Eulerian particle size method [19]. Zhang et al. designed a method to predict the sand concentration and volume fraction distribution of sand-oil flow in a horizontal pipeline, and conducted simulation studies using the Eulerian-Eulerian model [20]. Watcharasing et al. developed a prototype unit of advanced production separators for sand removal [21]. Ji et al. numerically modeled the rock chip particle distribution using CFD and discrete element dynamics to obtain a rock chip remover for horizontal wells with lower drilling costs and higher efficiency [22]. Zhou et al. investigated the solid-liquid two-phase hydrodynamic properties of horizontal wells through experiments and numerical simulations [23]. Nie et al.

experimentally determined the safety of downhole solid-liquid separators under torsion. They used numerical simulation methods to conduct modal analysis and erosion analysis of solid-liquid separators [24]. Skenderija et al. experimentally simulated the flow of fluid particles in a horizontal wellbore and derived different patterns of rock chip movement in the well [25]. Liang et al. designed a novel cyclone separator structure that can improve the separation efficiency of fine sand particles in downhole environments [26]. Ye et al. conducted an experimental study on the transport and settling of sand grains and derived the maximum settling rate of sand grains [27]. Wang et al. designed a novel downhole sand removal device that can improve production efficiency, providing a novel structural reference for current downhole sand removal devices [28]. The aforementioned studies have not considered the impact of certain parameters in the downhole environment on sand deposition and separation. Additionally, many current sand removal methods and devices have low sand removal efficiency. Therefore, it is necessary to innovate the design of sand removal device structures and to study and analyze various parameters that affect their separation performance.

In summary, the current sand removal technology for oil and gas wells faces many problems, such as low sand removal efficiency and limited sand removal methods. Therefore, a novel sand-bailing device is designed in this paper. The novelty of the novel sand-bailing device design lies in the use of a separation cover to internally separate sand and water, which is characterized by high separation efficiency and fast separation speed. The novel sand-bailing device was structurally designed and subjected to simulation analysis. The numerical simulation results were compared with experimental data, validating the accuracy and reliability of the numerical model. This comparison demonstrated the rationality of the structure and its ability to improve sand cleaning efficiency. Additionally, numerical simulations were conducted to analyze the key parameters affecting the separation efficiency, with the aim of optimizing these parameters to enhance the device's separation performance. The device aids in sand removal operations under complex downhole conditions, enabling efficient and rapid clearing of sand deposits in wells. It is especially beneficial for low-pressure, leakage-prone oil and gas wells, offering high operational efficiency.

ISSN: 2688-8645

2. System Design and Sand-liquid Separation Mechanism.

2.1. The Novel Sand-bailing Device System and Principle

In response to the production decrease caused by water and sand discharge, sand accumulation, and formation damage during downhole operations, a novel sand-bailing device has been designed based on existing sand dredging technology and requirements. The system scheme is illustrated in Figure 1.

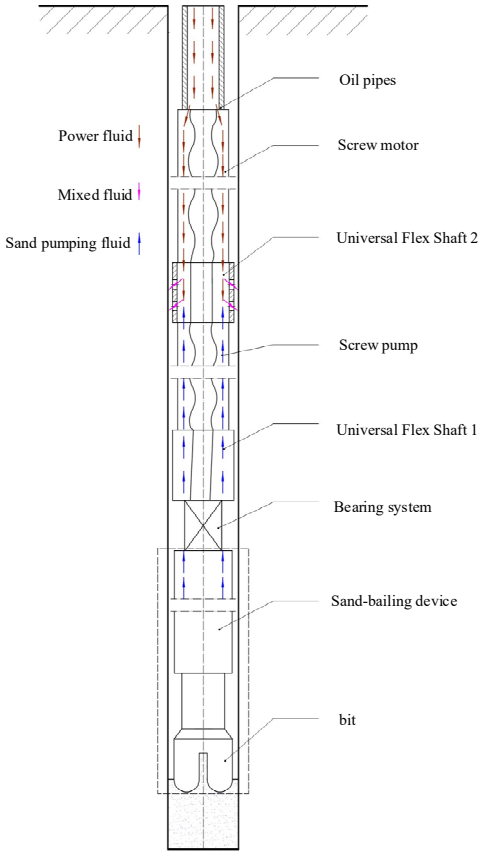

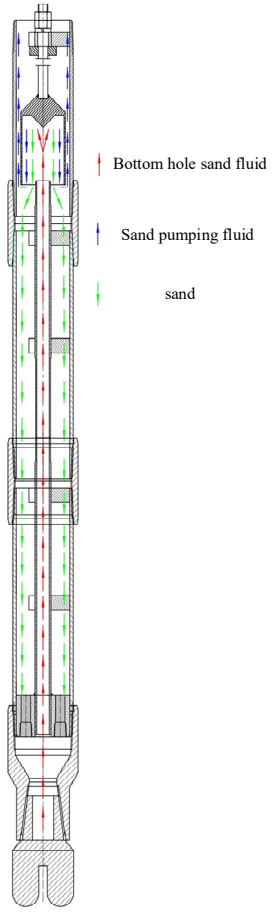

Figure 1. System diagram Figure **Figure 2.** Working principal diagram

The working principle of the novel sand-bailing device system is shown in Figure 1. High-pressure power fluid enters the bottom of the well through the central pipe of the double-layer continuous oil pipes. This fluid drives the rotational mechanical power generated by the screw motor and transfers it to the screw pump and sand-proof drilling bit through the universal flexible shaft. The sand-proof drilling bit rotates and agitates, crushing the bottom sediments to form a suspension of sand slurry. The bottom sand slurry enters the sand-bailing device through the central pipe of the double-layer oil pipes. The sand and water are separated by the separation cover inside the sand-bailing device. Under the force of gravity, the sand settles in the annular space of the sand-bailing device, while the sand slurry is drawn to the connection point and mixes with the low-pressure power fluid exiting the screw motor to form a mixed liquid. The mixed liquid is discharged to the bottom of the well through tiny holes on both sides of the connection point and then undergoes cyclic sand dredging in the system.

The separation principle of the sand-bailing device is illustrated in Figure 2. The bottom well sand slurry enters the separation device through the central pipe for sand-water separation. Once the sand slurry enters the separation cover, if the fluid velocity surpasses the free settling speed of sand particles, the sand slurry can undergo sand-water separation within the

ISSN: 2688-8645

separation cover. Due to gravity, the sand particles in the sand slurry settle to the bottom of the sand-bailing device. A small portion of the sand-containing slurry is drawn to the connection point by the power provided by the motor pump and mixed with the low-pressure power fluid. The mixed liquid is then discharged into the bottom of the well. Figure 3a illustrates the sand particle transport and sedimentation processes within the sand-bailing cylinder. The sand scooping cylinder is the core part of the novel sand-bailing device, capable of achieving sand-water separation. Figure 3b is a block diagram of the interior of the sand scoop cylinder. There are four major areas in the cylinder: the sand transport area, the sand settling area, the sand-water mixing area and the sand storage area. After the sand particles and liquid are separated by the sand-bailing cylinder at the bottom of the well, the sand particles enter the settling area. The settled sand particles then move into the sand storage area, thereby completing the sand-water separation.

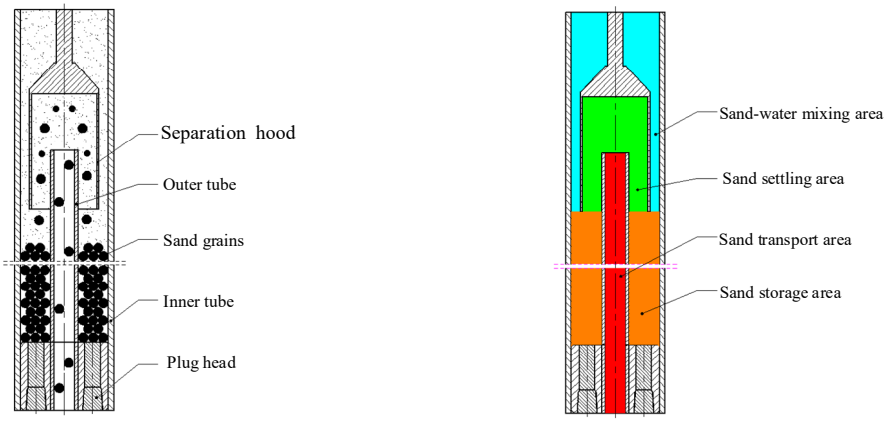

(a) Sand particle transport flowchart (b) Structural partition diagram

Figure 3. Schematic diagram of the principle of sand removal

2.2. Structural Design of the Novel Sand-bailing Device

The structural principles of the novel sand-bailing device are illustrated in Figure 4, and its structural design and optimization have been conducted.

The sand dredging structure in the novel sand-bailing device system has been simplified, as shown in Figure 5 after simplification. The simplified model allows for localized improvements to analyze the most suitable structure for sand dredging, aiming to determine the design that yields the optimal separation efficiency.

Based on the preliminary design of the structural schematic diagram of the novel sand-bailing device, three types of sand-bailing devices have been initially designed, as shown in Figure 6. Among them, Figure 6a represents the Single-Cone Separation (SCS) sand-bailing device, Figure 6b represents the Double-Cone Separation (DCS) sand-bailing device, and Figure 6c represents the Cone-Less Separation (CLS) sand-bailing device.

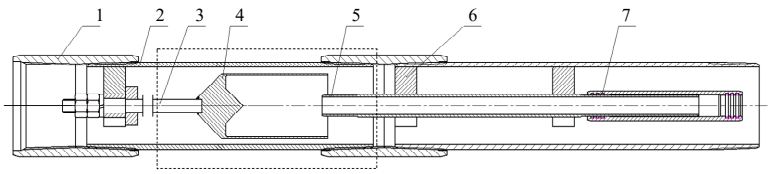

1. Tubing coupling; 2. Tube; 3. Separation cover rod; 4. Separation cover; 5. Central tube; 6. Fixed medium plate; 7. Docking sealing pipe

Figure 4. Schematic diagram of the structural principles of the novel sand-bailing device

ISSN: 2688-8645

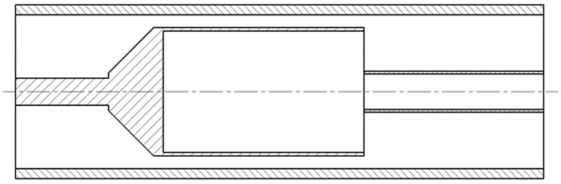

Figure 5. Simplified diagram of the structure of the novel sand-bailing device

(a) SCS (b) DCS (c) CLS

Figure 6. Diagram of the three proposed models

3. Numerical Simulation

3.1. Calculation Model and Boundary Conditions

The Eulerian multiphase flow model was selected for the calculations, as it can provide a certain level of accuracy in simulating flow velocity and separation efficiency. The Euler method considers each phase as a continuous medium that fills the entire flow field, with solid-phase particles permeating the fluid as a continuous medium or pseudo-fluid. [29]. The turbulence model used for the simulation is the standard k-ε model due to the presence of effects such as rotationality and viscosity [30, 31].

This paper uses a three-dimensional model and a transient double precision implicit solver. The calculation algorithm uses the SIMPLE algorithm, which is suitable for pressure-velocity coupling [32]. The wall employs standard wall functions, with no-slip and impermeable boundary conditions. Table 1 provides the boundary conditions and material properties for the medium. The time step is 0.001 s, and the convergence accuracy is set to 10−6.

Table 1. Boundary conditions and physical parameters of the medium

name		numerical value
Velocity-Inlet-		0.8 m/s
Outlet	overflow	outflow
	underflow	
water	density	1000 kg/m³
	viscosity	0.001 Pa·s
	volume fraction	80%
	diameter	-
sand	density	2500 kg/m³
	viscosity	-
	volume fraction	20%
	diameter	0.2 mm

ISSN: 2688-8645

The computational equations used for numerical simulations with the Euler model can be simulated using the three main governing equations and the standard model equations derived by previous researchers [33].

Continuity equation:

$$\frac{\partial}{\partial t}(\rho_\alpha \phi_\alpha) + \nabla \cdot (\rho_\alpha \phi_\alpha \mu_\alpha) = \nabla \cdot (\alpha_\alpha J_\alpha) + \dot{m}_a \quad (1)$$

Momentum equation:

$$\frac{\partial}{\partial t}(\rho_\alpha \mu_\alpha) + \nabla \cdot (\rho_\alpha \mu_\alpha \mu_\alpha) = -\nabla p + \nabla \cdot \tau_\alpha + f_\alpha \quad (2)$$

Energy conservation equation:

$$\frac{\partial}{\partial t}(\rho_\alpha E_\alpha) + \nabla \cdot (\rho_\alpha \mu_\alpha E_\alpha) = -\nabla \cdot q_\alpha + \nabla \cdot (\tau_\alpha \cdot \mu_\alpha) + \dot{Q}_\alpha \quad (3)$$

Standard k−ε model equations:

Turbulent Kinetic Energy Equation (k Equation):

$$\frac{\partial}{\partial t}(\rho k) + \nabla \cdot (\rho k u) = \nabla \cdot \left[\left(\mu + \frac{\mu_l}{\sigma_k} \right) \nabla k \right] + P_k - \rho \varepsilon \quad (4)$$

Dissipation Rate Equation (ε Equation):

$$\frac{\partial}{\partial t}(\rho \varepsilon) + \nabla \cdot (\rho \varepsilon u) = \nabla \cdot \left[\left(\mu + \frac{\mu_t}{\sigma_\varepsilon} \right) \nabla \varepsilon \right] + C_1 \frac{\varepsilon}{k} P_k - C_2 \rho \frac{\varepsilon^2}{k} \quad (5)$$

3.2. Geometric Model and Grid Independence Study

A three-dimensional fluid domain model of the novel sand-bailing device was created using 3D software. Its basic structure consists of the overflow, separation hood rod section, separation hood section, inlet pipe section, inlet, and underflow. The three-dimensional model and the planar structure diagram of the novel sand-bailing device are shown in Figure 7, and the specific design parameters are detailed in Table 2.

Table 2. Design parameters of the novel sand-bailing device

Name	Sign	Dimension(mm)
Outer flow tube inner diameter	D	90.1
Separation hood inner diameter	D1	71
Inlet pipe inner diameter	D2	21
Separation hood rod diameter	D3	22
Separation hood cone end diameter	D4	16
Outer flow tube length	L	310
Inlet pipe length	L1	105.4
Separation hood outer length	L2	123.5
Separation hood rod length	L3	54.6
Separation hood inner length	L4	118

A novel sand-bailing device with a single inlet and dual outlets was designed for downhole practical conditions. The Mesh module included in ANSYS was utilized to partition the mesh for the three-dimensional model of the novel sand-bailing device. Tetrahedral meshing was used, and the computational mesh of 635,692 cells is shown in Figure 8. The number of grid cells significantly impacts the accuracy of the calculation results. Different numbers of grid cells were chosen to verify grid independence. Table 3 shows the validation of grid independence for separation efficiency with a maximum error of 0.19%. Figure 9 shows the radial velocity distribution at Z = 100 mm for five different mesh numbers. The radial velocities of grid cell

ISSN: 2688-8645

numbers 635,692 and 785,071 are relatively consistent. Therefore, when the number of grid cells exceeds 635,692, the separation efficiency and radial velocity obtained are independent of the number of grid cells. The numerical model results studied in this paper can be determined to be independent of the mesh, meaning the results are mesh-independent. To save computation time while ensuring calculation accuracy, a mesh with 635,692 elements can be selected for numerical analysis.

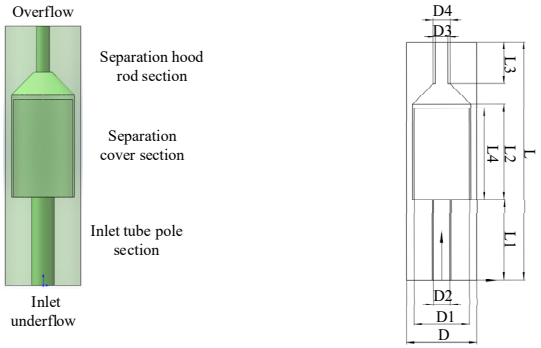

Figure 7. Three-dimensional model and planar structural diagram

Table 3. Independent verification of separation efficiency.

Total number of cells	Separation efficiency (%)
382848	82.38
448063	82.31
534373	82.28
635692	82.22
785071	82.19
Difference (%)	0.19

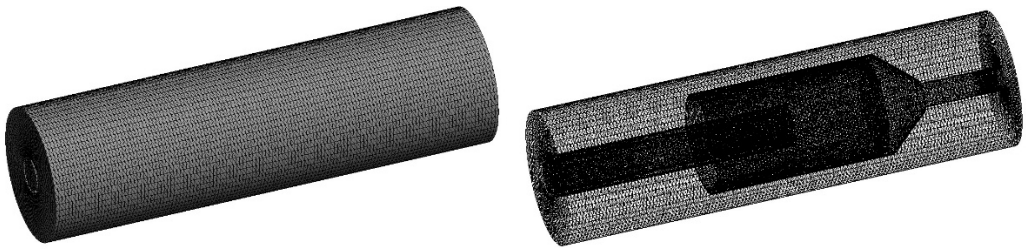

(a) (b)

Figure 8. The computational grids of the 635,692 cells (a: external mesh diagram; b: internal mesh diagram)

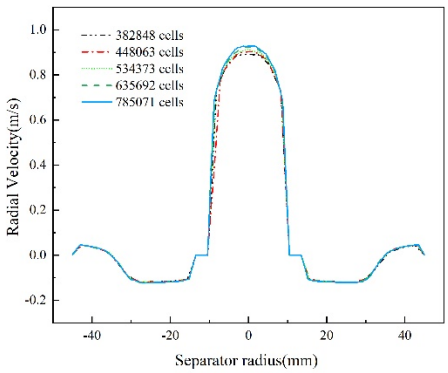

Figure 9. Radial velocity at Z = 100mm under five different mesh numbers.

ISSN: 2688-8645

3.3. Definition of Separation Efficiency and Structural Optimization

Separation efficiency is a crucial indicator of the performance of a sand-bailing device. The device studied in this paper has a single inlet and dual outlets. From a purification perspective, separation efficiency is defined as the percentage of sedimented sand phase at the overflow, which can be calculated using the following formula:

$$E = \frac{q_u}{q_i} \times 100\% \quad (6)$$

In the formula, q_u is the mass flow rate of the sand phase at the underflow, q_i is the mass flow rate of the sand phase at the inlet, and E is the separation efficiency.

The mass flow rates are reported under "Reported-Fluxes." The separation efficiency of the sand-bailing device is determined by dividing the mass flow rate of the sand phase at the underflow by the mass flow rate at the inlet, with the residual value representing the simulation error . The calculated results for the mass flow rate and separation efficiency at the inlet, overflow, and underflow are presented in Table 4.

Table 4. Simulation results of three types of sand-bailing devices

Structure type	Sand phase mass flow rate (kg·s^{-1})			Differentials (kg·s^{-1})	Separation efficiency (%)
	overflow	inlet	underflow		
SCS	-0.0217	0.1372	-0.1129	0.0026	82.27
DCS	-0.0217	0.1371	-0.1127	0.0027	82.22
CLS	-0.0274	0.0548	-0.0274	0.0001	50.00

Taking into account both structural design and separation performance, the Single-Cone Separation (SCS) sand-bailing device is chosen for its structural simplicity, ease of fabrication, and efficient separation capability. Following this selection, the key dimensional parameters of the SCS device will be further optimized. Additionally, a negative sign ("-") is used to indicate outflow.

4. Results and Discussion

4.1. Validation of the Numerical Model

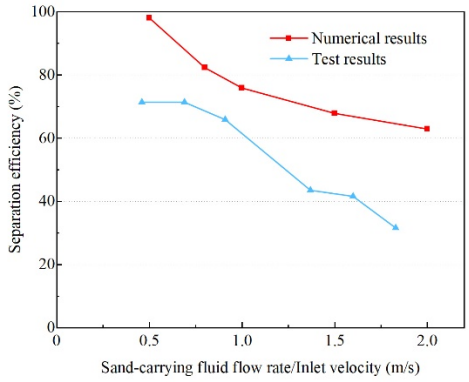

Figure 10. Comparison of numerical results with test results

To ensure the reliability of the computational model, the simulation results of the novel sand-bailing device are compared with the test results from Ye [27], as shown in Figure 10. The results show that the numerical simulation results exhibit the same trend as the test results, with the separation efficiency of sand particles decreasing gradually with the inlet flow rate.

ISSN: 2688-8645

Due to the inclusion of the separation hood, the simulation results show higher separation efficiency than the experimental results, indicating that the computational model presented in this paper can simulate the separation performance of the novel sand-bailing device with reasonable accuracy and reliability. Therefore, the Euler multiphase flow model and the standard k-ε turbulence model are effectively applied to the novel sand-bailing device.

4.2. Optimization of Inlet Tube Length and Separation Hood Structure

Simulation Conditions: The structural dimensions are the same as those in the initial design, and numerical simulations are conducted on four groups of sand-bailing devices with different inlet pipe lengths. The inlet velocity is 0.8 m/s, the volume percentage of sand is 20%, the sand particle size is 0.2 mm, and the liquid viscosity is 1 mPa·s. Simulations and analyses are carried out under the conditions of inlet pipe lengths of 105.4 mm, 113.4 mm, 165.4 mm, and 195.4 mm, with a comparison of different inlet pipe lengths shown in Figure 11. Figure 12 shows that when the inlet pipe length is 165.4 mm, the separation efficiency is relatively high, reaching 82.3%. Furthermore, as the inlet pipe length increases, the separation efficiency of the novel sand-bailing device initially increases and then decreases, but the overall change is minimal.

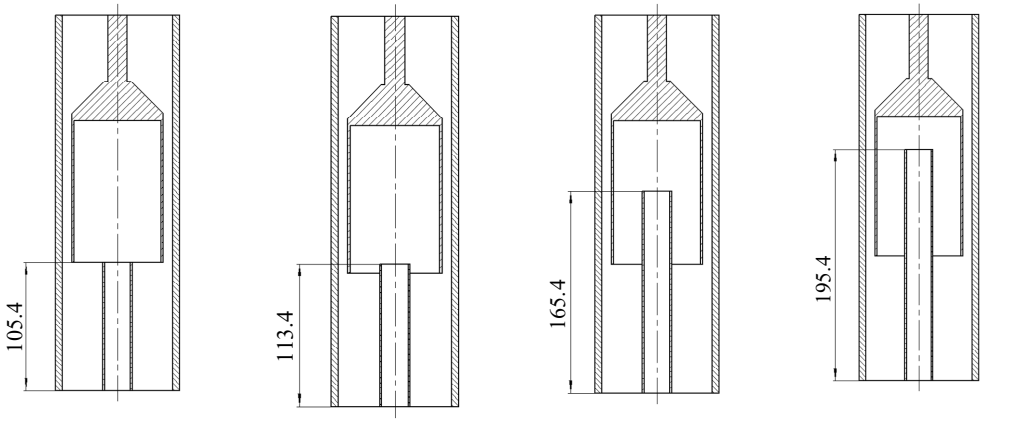

(a) L=105.4mm (b) L=113.4mm (c) L=165.4mm (d) L=195.4mm

Figure 11. Structure diagrams of different inlet pipe lengths

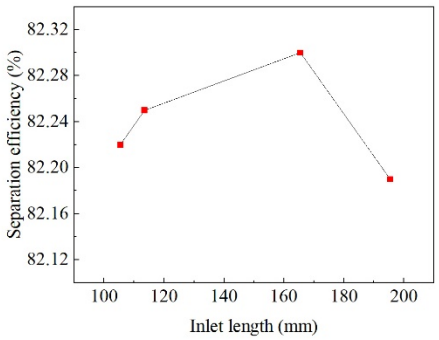

Figure 12. The impact of inlet pipe diameter variation on separation efficiency

Keeping other structural parameters unchanged, the inlet pipe length is set to the simulated result of 165.4 mm. Numerical simulations are conducted for different separation hood diameters: 59 mm, 63 mm, 67 mm, and 71 mm. A comparison of different separation hood diameters is shown in Figure 13 From Figure 14, it can be observed that as the separation hood diameter changes, the separation efficiency of the sand-bailing device initially increases, then decreases, and finally stabilizes. The separation efficiency is highest with a separation hood

ISSN: 2688-8645

diameter of 63 mm, reaching 88.93%. Therefore, selecting a separation hood diameter of 63 mm provides the best separation efficiency for the sand-bailing device.

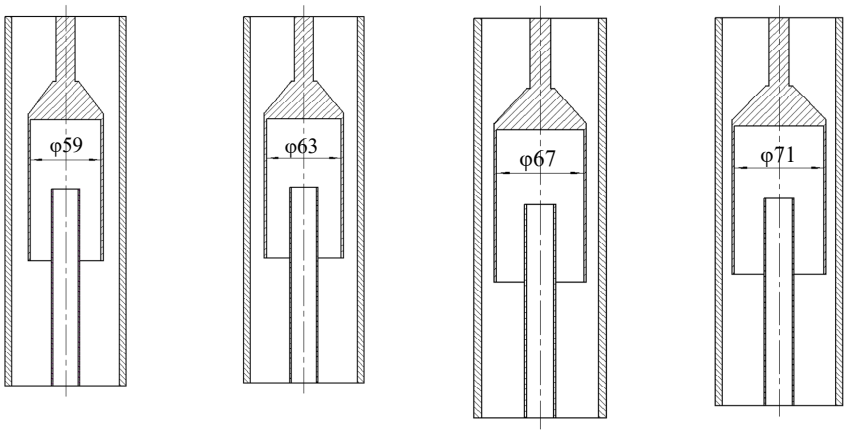

(a)φ59mm (b)φ63mm (c)φ67mm (d)φ71mm

Figure 13. Structural diagrams of different separation hood diameters

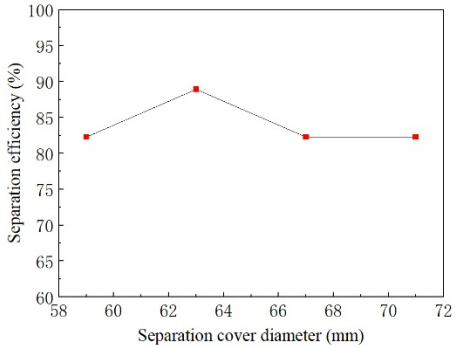

Figure 14. The impact of separation hood diameter variation on separation efficiency

4.3. The Effect of Drilling Speed and Inlet Flow Rate on Separation Efficiency

The volume fraction of sand is related to the drilling speed. As the drilling speed increases, the volume fraction of sand also increases, and vice versa. The corresponding relationship between drilling speed and the volume fraction of sand is shown in Table 5, and the impact of drilling speed variations on the separation efficiency is illustrated in Figure 15.

Table 5. The correspondence between drilling speed and the volume fraction of sand

Drilling speed (m/h)	Sand phase volume fraction(%)	Sand phase inlet mass flow rate (kg·s^{-1})
4.07	5	0.0342
8.18	10	0.0686
12.22	15	0.1025
16.36	20	0.1372
20.37	25	0.1708

Table 5 shows that as the drilling speed increases, the volume fraction of the sand phase becomes more significant, and the inlet mass flow rate of the sand phase also increases. From Figure 15, it can be seen that as the drilling speed increases, the separation efficiency of the sand-bailing device exhibits a decreasing trend. At the same drilling speed, a larger inlet mass flow rate results in a more pronounced decrease in separation efficiency and a lower overall separation efficiency. Simulation analysis reveals that when the drilling speed does not exceed 16.5 m/h, the separation efficiency of the sand-bailing device exceeds 80%. Therefore, selecting

ISSN: 2688-8645

a suitable drilling speed within this range allows for optimal sand-catching capacity and separation efficiency of the sand-bailing device. Additionally, it is advisable to control the inlet mass flow rate of the sand phase within a specific range to ensure a high drilling speed and sufficient separation efficiency, thus preventing sand burial accidents in the sand-catching system. The simulated analysis results provide valuable data guidance and practical parameters for subsequent experimental verification.

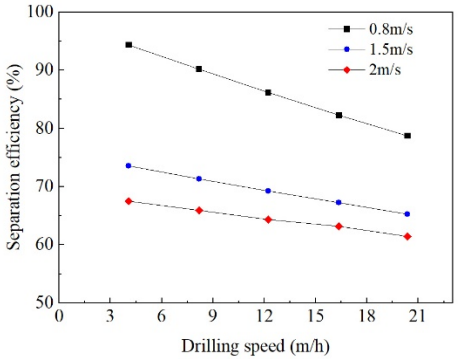

Figure 15. The impact of drilling speed variations on separation efficiency

As shown in Figure 16, at a certain drilling speed, the separation efficiency gradually decreases as the inlet speed increases, with the magnitude of the decrease also becoming larger. At the same inlet speed, a larger drilling speed results in a similar trend in the separation efficiency of the sand filter, but with a lower overall separation efficiency. When the flow rate at the inlet pipe is low, there is a possibility that, at a certain velocity, sand particles in the pumped liquid may directly sink from the inlet, affecting the separation of sand and liquid. The sand-catching capacity increases with higher pump suction flow rates. However, under constant cross-sectional area conditions, an increase in flow rate corresponds to an increase in velocity. The higher the velocity, the lower the separation efficiency of the sand-liquid mixture. This contradiction necessitates a comprehensive consideration of both sand-catching performance and separation efficiency. Therefore, selecting an appropriate suction flow rate, which involves choosing a suitable screw pump, becomes essential.

Table 6. The flow velocity at the inlet pipe and the pump suction flow rate

The inner diameter of the inlet pipe (mm)	The flow velocity at the inlet pipe (m/s)	The pump suction flow rate (L/min)
21	0.5	10.4
21	0.75	15.6
21	1	20.8
21	1.5	31.2
21	2	41.6
21	2.5	52.0

Based on the simulation curve in Figure 16, it can be determined that the appropriate inlet velocity for sand with a particle size of 0.2 mm is between 0.75 and 1.2 m/s. Within this range, the separation efficiency of the sand-water mixture exceeds 70%. By selecting an appropriate inlet velocity within this range, suitable flow rate parameters for the pump can be determined, allowing for the selection of a screw pump with high sand-catching capacity and high separation efficiency. Table 6 shows the changes in pump suction flow rate under different flow velocities. The research results provide data references for the subsequent selection of an appropriate

ISSN: 2688-8645

screw pump. A comparison with other literature reveals that the flow influence pattern is consistent with the study in this paper, and the appropriate flow range is similar [27].

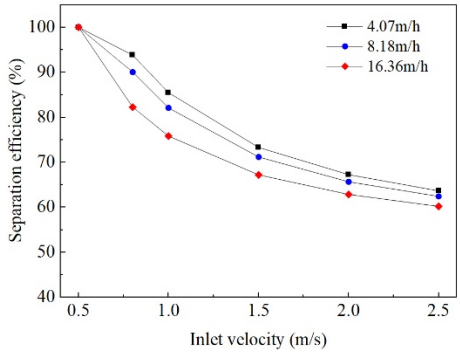

Figure 16. Effect of inlet velocity on separation efficiency

4.4. The Effect of Sand Particle Size and Drilling Fluid Viscosity on Separation Efficiency

From Figure 17, it can be observed that as the sand particle size decreases, the force exerted by the flow field on the particles also decreases. Consequently, more sand particles are carried out through the upper outlet, while smaller particles are not discharged from the bottom outlet. Instead, smaller particles are carried along with the water phase through the upper outlet. As the sand particle size increases, these phenomena become less significant, and the separation efficiency of the sand-bailing device gradually improves. For the same sand particle size, the greater the viscosity of the well fluid, the lower the separation efficiency.

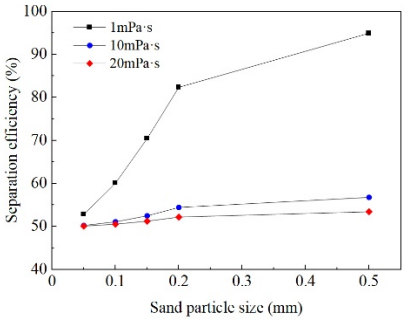

Figure 17. The impact of sand particle size variations on separation efficiency

The research results indicate that the sand-bailing device achieves higher separation efficiency, exceeding 70%, when the sand particle size is larger than 0.15 mm. Therefore, the sand-bailing device designed in this paper is more suitable for separating sand particles with a diameter greater than 0.15 mm. However, when the sand particle size is too large, it may cause pipeline blockage. In such cases, it is necessary to crush the sand particles to reduce their size before further separation processing.

The variation in drilling fluid viscosity alters the velocity field, pressure field, turbulent flow field, and distribution pattern of the sand phase within the sand-bailing device, ultimately causing changes in the sand-bailing device's separation efficiency. From Figure 18, it can be observed that as the drilling fluid viscosity increases, the separation efficiency of the sand-bailing device shows a decreasing trend. At the same velocity, higher drilling fluid viscosity increases internal frictional resistance and results in a more significant loss of fluid kinetic energy, leading to a sharp decrease in fluid velocity, thereby affecting the sand-bailing device's separation performance. At the same well-fluid viscosity, the separation efficiency of the sand trap improves with the sand-bailing devices.

ISSN: 2688-8645

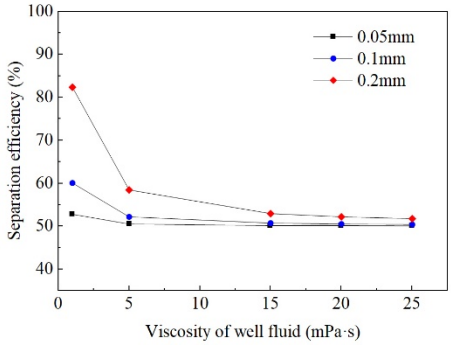

Figure 18. The impact of drilling fluid viscosity variations on separation efficiency.

Based on the above analysis, it is evident that under a certain inlet flow velocity, there is an appropriate range of drilling fluid viscosity for downhole sand-bailing devices. For a sand particle size of 0.2 mm and at an inlet velocity of 0.8 m/s, the sand-bailing device is suitable for separating fluids with a viscosity not exceeding 2 mPa·s. In this range, the separation efficiency is greater than 70%, which satisfactorily meets the requirements for oilfield fluid-sand separation.

5. Summary

In this paper, the separation performance of the novel sand-bailing device is investigated under different working parameters. The comparison of the numerical simulation results with the test results reveals the same change trend, which confirms the reliability of the numerical calculation model. By applying a single-factor method, the optimal structural parameters for the sand-bailing device are determined. The optimal inlet pipe length is 165.4 mm, and the separation hood diameter is 63 mm. As the drilling speed and inlet flow rate increase, the separation efficiency of the sand-bailing device shows a decreasing trend. The optimal drilling speed should not exceed 16.5 m/h, and the suitable inlet velocity ranges from 0.75 to 1.2 m/s, ensuring that the separation efficiency of the sand dredger remains above 70%. The separation efficiency of the sand-bailing device increases with the increase in sand particle size, and it exhibits good separation performance for sand particles with a diameter greater than 0.15 mm, with a separation efficiency exceeding 70%. The separation efficiency of the sand-bailing device decreases with the increase in drilling fluid viscosity. When the liquid viscosity exceeds 5 mPa·s, the separation efficiency is less affected by the viscosity. The sand-bailing device is suitable for separating fluids with a viscosity not exceeding 2 mPa·s, with the separation efficiency exceeding 70%. This study provides a novel scheme and research method for the structural design of the novel sand-bailing device and the factors influencing the separation efficiency.

References

[1] Bo, J., et al. Study on sand production and management of periodic injection wells in eastern transition zone. AIP Conference Proceedings. 9 November 2018, p. 030046.

[2] Wang, D.Y. Causes of sand production in oil wells and application of sand control technology. Chemical Engineering Management. 2019, Vol. (No. 02), p. 200-201.

[3] Li, H.H. Harm of sand production in oil wells and analysis of sand control technology. West-China Exploration Engineering. 2021, Vol. 33 (No. 04), p. 95-96.

[4] Coffee, S., Briffett, et al. Downhole desander prevents ESP damage in high-water cut well. World Oil. 2008, Vol. 229 (No. 6).

[5] Hu, C.: Research on Regularity of Sand Particle Migration in Horizontal and Sand Cleaning Devices (Thesis, Yangtze University, China 2020). p.42.

[6] Chen, Y.L. Complex prevention and control and disposal of wellbore sand and drilling cuttings deposition accidents. Chemical Engineering Management. 2018, Vol. 484 (No. 13), p. 78.

[7] Zhang, J., Yuan, H., Cheng, L., et al. Inverse estimation of the sand concentration for sand-oil flow in a horizontal pipeline based on the Eulerian–Eulerian model. Journal of Petroleum Science and Engineering. 2020, Vol. 195, p. 107877.

[8] Wang, J., Xie, B., Luo, X., et al. Successful Application of the Sand Removal Technique by Use of Concentric Tubing Jet Pump in Karamay Shallow Heavy Oil. Society of Petroleum Engineers. 2010.

[9] Medina, N., Pdvsa, J.D., Pachon, L., et al. Application of concentric coiled-tubing and well-vacuuming device with chemical sand-consolidation resins for controlling sand production in wells with damaged screens or slotted liners: A Rig less Well-repair Alternative. SPE Latin American and Caribbean Petroleum Engineering Conference.

[10] Gunther, O., Higgins, G., Li, J., et al. Ultra-Low Pressure Wellbore Cleanouts Using Micro-vacuuming Technology and Concentric Coiled Tubing. Society of Petroleum Engineers. Doha, 2009.

[11] Li, J., Green, T., et al. Coiled Tubing Sand Cleanouts Utilize BHA Technology and Simulation Software in Demanding Wellbore Geometries. Society of Petroleum Engineers. Al-Khobar, 2018.

[12] Li, J., Misselbrook, J., Sach, M., et al. Sand Cleanouts with Coiled Tubing: Choice of Process, Tools and Fluids. Journal of Canadian Petroleum Technology. 2010, Vol. 49 (No. 8), p. 69-82.

[13] Liu, C.-L., Shi, M.-H., Dai, P.-S., et al. The motion of solid particles in a tube's vertical upward flow field. J. Pet. Univ. (Nat. Sci. Ed.). 1998, Vol. 10, p. 82–86.

[14] Li, M.Z., Wang, W.Y., He, Y.F., et al. Study the sand-carrying rule of vertical wellbore. J. Pet. Univ. (Nat. Sci. Ed.). 2000, Vol. 24 (No. 2), p. 33–43.

[15] Li, M.Z., Wang, W.Y., Zhao, G.J., et al. Study the flow law of sand carried by vertical wellbore fluid and its application in oil and gas well production. Exp. Mech. 2002, Vol. 17 (No. 3), p. 385–392.

[16] Park, Y.-C., Yoon, C.-H., Lee, D.-K., Kwon, S.-K., et al. Design of Hydrocyclone For Solid Separation. Sixth ISOPE Ocean Mining Symposium. Changsha, Hunan, China, October 2005.

[17] Severino, J.G., Gomez, L.E., Wang, S., Mohan, R.S., Ovadia Shoham, et al. Mechanistic Modeling of Solids Separation in Solid/Liquid Hydrocyclones. SPE Proj Fac & Const. 2010, Vol. 5, p. 121–135.

[18] Huang, Q., Liu, Q., Zang, S., et al. Three Dimensional Numerical Simulation of Solid-liquid Separation of Horizontal Spiral Sedimentation Centrifuge. Advances in Chemical, Material and Metallurgical Engineering, Pts 1–5, p. 1655–1658.

[19] Kamyab, M., Rasouli, V., et al. Experimental and numerical simulation of cuttings transportation in coiled tubing drilling. Journal of Natural Gas Science and Engineering. 2016, Vol. 29, p. 284–302.

[20] Zhang, X., Liu, Z., Wang, D., Liu, T., Zhang, J., Ll, D., Gao, Z., Xu, Q., et al. Low Damage Negative Pressure Sand-bailing Technology for CBM Horizontal Wells. Coal Technology. 2020, Vol. 39 (No. 12), p. 32–34.

[21] Watcharasing, S., Lamsunthia, S., Phuphuak, Y., Malatip, A., Pratumwal, Y., Kiattikomol, P., et al. Smart Facility Advanced Separator. International Petroleum Technology Conference. Virtual, March 2021.

[22] Ji, G., Wang, H., Huang, H., Meng, Z., Cui, L., Guo, W., et al. Design and test of a cuttings bed remover for horizontal wells. Natural Gas Industry B. 2021, Vol. 8 (No. 4), p. 412–419.

[23] Zhou, Y.J., He, Y.F., Li, Z.J., Ju, G.S., et al. Hole Cleaning Performance of V-Shaped Hole Cleaning Device in Horizontal Well Drilling: Numerical Modeling and Experiments. Applied Sciences-Basel. 2022, Vol. 12 (No. 10).

[24] Nie, Q., Zhang, S., Huang, Y., Yi, X., Wu, J., et al. Numerical and Experimental Investigation on Safety of Downhole Solid-Liquid Separator for Natural Gas Hydrate Exploitation. Energies. 2022, Vol. 15 (No. 15).

[25] Skenderija, J., Koulidis, A., Sanchez, D.L., Ahmed, S., et al. Advanced Hole Cleaning in Horizontal Wells: Experimental Investigation Supported by a Downhole Clamp-On Tool. Middle East Oil, Gas and Geosciences Show. p. D021S062R002.

ISSN: 2688-8645

[26] Liang, H.Z., Jian, M., Li, C.Z., Liu, M., Jiang, X.K., et al. Study on the performance of downhole axial cyclone with spiral fins for drainage and sand removal. Journal of Environmental Chemical Engineering. 2023, Vol. 11 (No. 5), p. 111032.

[27] Ye, Z., Zhao, Y., Pang, Y., Hu, Y., Jiang, Q., et al. Mechanisms and Experimental Research on Sand Transport and Settlement of a New Sand Cleaning System. Arabian Journal for Science and Engineering. 2023, Vol. 48 (No. 12), p. 16543–16555.

[28] Wang, Z.L., Fang, Z.G., Wang, Z.S., Zhang, M.L., Liao, R.Q., et al. Improvement of sand-washing performance and internal flow field analysis of a novel downhole sand removal device. Scientific Reports. 2024, Vol. 14 (No. 1), p. 15482.

[29] Cader, T., Masbernat, O., Rocom, C., et al. Two-phase velocity distributions and overall performance of a centrifugal slurry pump. Journal of Fluids Engineering. 1994, Vol. 116 (No. 2), p. 316–323.

[30] Lam, C.K.G., Bremhorst, K., et al. A modified form of the k–ε model for predicting wall turbulence. Journal of Fluids Engineering. 1981, Vol. 103 (No. 3), p. 456–460.

[31] Goodarzi, M., Safaei, M.R., Vafai, K., Ahmadi, G., Dahari, M., Kazi, S.N., Jomhari, N., et al. Investigation of nanofluid mixed convection in a shallow cavity using a two-phase mixture model. International Journal of Thermal Sciences. 2014, Vol. 75, p. 204–220.

[32] Van Doormaal, J.P., Raithby, G.D., et al. Enhancements of the SIMPLE method for predicting incompressible fluid flows. Numerical Heat Transfer. 1984, Vol. 7 (No. 2), p. 147–163.

[33] Hargreaves, D.M., Wright, N.G., et al. On the use of the k–ε model in commercial CFD software to model the neutral atmospheric boundary layer. Journal of Wind Engineering and Industrial Aerodynamics. 2007, Vol. 95 (No. 5), p. 355–369.